Supplementary Material (ESI) for Chemical Communications

The role of temperature on the structure and dimensionality of MOFs: An illustrative study of the formation of Manganese Oxy-bis(benzoate) structures

Partha Mahata,[a] A. Sundaresan[b] and Srinivasan Natarajan[a*]

[a] Framework Solids Laboratory, Solid State and Structural Chemistry Unit, Indian Institute of Science, Bangalore 560 012, India E-mail: snatarajan@sscu.iisc.ernet.in

[b] *Chemistry and Physics of Material Unit, Jawaharlal Nehru Centre For Advanced Scientific Research, Bangalore-560064, India*

ELECTRONIC SUPPLEMENTARY INFORMATION

Table S1: Crystal data and structure refinement parameters for $[\{Mn(H_2O)_3\}\{C_{12}H_8O(COO)_2\}].H_2O$, **I**, $[\{Mn(H_2O)\}\{C_{12}H_8O(COO)_2\}]$, **II,** and $[\{Mn(OH)\}_2\{C_{12}H_8O(COO)_2\}]$, **III**

Structure parameter	**I**	**II**	**III**
Empirical formula	$C_{14}H_{16}O_9Mn$	$C_{14}H_{10}O_6Mn$	$C_{14}H_{10}O_7Mn_2$
Formula weight	383.19	329.16	400.1
Crystal system	Monoclinic	Monoclinic	Orthorhombic
Space group	$P2_1/c$ (no. 14)	P2/c (no. 13)	Pnca(no. 60)
a (Å)	16.902(6)	14.399(3)	29.135(8)
b (Å)	10.506(4)	6.3626(15)	7.461(2)
c (Å)	9.062(3)	7.3555(18)	6.1111(17)
α (deg)	90.0	90.0	90.0
β (deg)	94.524(5)	102.867(4)	90.0
γ (deg)	90.0	90.0	90.0
Volume ($Å^3$)	1604.2(9)	657.0(3)	1328.4(6)
Z	4	2	4
T (K)	273(2)	293(2)	293(2)
ρ_{calc} (g cm^{-3})	1.578	1.664	2.001
μ (mm^{-1})	0.868	1.030	1.938
θ range (deg)	2.28 to 28.03	2.90 to 28.02	2.80 to 27.97
λ (Mo Kα) (Å)	0.71073	0.71073	0.71073
R indices [I>2σ(I)]	R_1 = 0.0444, wR_2 = 0.1133	R_1 = 0.0384, wR_2 = 0.0814	R_1 = 0.0665, wR_2 = 0.1183
R indices (all data)	R_1 = 0.0511, wR_2 = 0.1180	R_1 = 0.0524, wR_2 = 0.0868	R_1 = 0.0893, wR_2 = 0.1243

$R_1 = \Sigma \, ||F_0|-|F_c|| \, / \, \Sigma \, |F_0|$; $wR_2 = \{\Sigma[w(F_0^2 - F_c^2)^2] \, / \, \Sigma[w(F_0^2)^2]\}^{1/2}$. $w = 1/[\sigma^2(F_0)^2 + (aP)^2 + bP]$, $P = [\max.(F_0^2,0) + 2(F_c)^2]/3$, where a = 0.0538 and b =2.3088 for **I**, a = 0.0414 and b = 0.0115 for **II** and a = 0.0224 and b = 6.7647 for **III**

Table S2: Selected bond distances (Å) observed in $[\{Mn(H_2O)_3\}\{C_{12}H_8O(COO)_2\}].H_2O$, **I**, $[\{Mn(H_2O)\}\{C_{12}H_8O(COO)_2\}]$, **II,** and $[\{Mn(OH)\}_2\{C_{12}H_8O(COO)_2\}]$, **III**

Bond	Distances, Å	Bond	Distances, Å
I			
Mn(1)-O(1)	2.1244(17)	Mn(1)-O(4)	2.1925(19)
Mn(1)-O(2)#1	2.1306(19)	Mn(1)-O(5)	2.218(2)
Mn(1)-O(3)#2	2.1666(19)	Mn(1)-O(6)	2.2511(18)
II			
Mn(1)-O(1)#1	2.0777(19)	Mn(1)-O(3)#3	2.1783(18)
Mn(1)-O(1)#2	2.0777(19)	Mn(1)-O(3)	2.1783(18)
Mn(1)-O(2)	2.105(3)		
III			
Mn(1)-O(1)#1	2.143(3)	Mn(1)-O(2)	2.223(4)
Mn(1)-O(1)	2.152(3)	Mn(1)-O(3)#3	2.248(3)
Mn(1)-O(1)#2	2.180(3)	Mn(1)-O(3)#1	2.275(3)

Symmetry operations used to generate equivalent atoms for **I**: #1 x,-y+1/2,z-1/2 #2 -x,-y,-z+1; for **II**: #1 x,-y+1,z-1/2 #2 -x+1,-y+1,-z+2 #3 -x+1,y,-z+3/2; for **III**: #1 -x+1,y+1/2,-z+1/2 #2 -x+1,-y,-z #3 -x+1,-y,-z+1

Table S3: Selected bond angles observed in $[\{Mn(H_2O)_3\}\{C_{12}H_8O(COO)_2\}].H_2O$, **I**, $[\{Mn(H_2O)\}\{C_{12}H_8O(COO)_2\}]$, **II,** and $[\{Mn(OH)\}_2\{C_{12}H_8O(COO)_2\}]$, **III**

Angle	Amplitude (º)	Angle	Amplitude
I			
O(1)-Mn(1)-O(2)#1	98.40(8)	O(3)#2-Mn(1)-O(5)	170.35(8)
O(1)-Mn(1)-O(3)#2	91.66(7)	O(4)-Mn(1)-O(5)	85.54(8)
O(2)#1-Mn(1)-O(3)#2	89.38(8)	O(1)-Mn(1)-O(6)	87.31(7)
O(1)-Mn(1)-O(4)	171.81(7)	O(2)#1-Mn(1)-O(6)	174.16(7)
O(2)#1-Mn(1)-O(4)	89.11(7)	O(3)#2-Mn(1)-O(6)	91.71(7)
O(3)#2-Mn(1)-O(4)	85.11(7)	O(4)-Mn(1)-O(6)	85.27(7)
O(1)-Mn(1)-O(5)	97.92(8)	O(5)-Mn(1)-O(6)	89.91(8)
O(2)#1-Mn(1)-O(5)	88.08(9)		
II			
O(1)#1-Mn(1)-O(1)#2	140.92(13)	O(2)-Mn(1)-O(3)#3	87.45(5)
O(1)#1-Mn(1)-O(2)	109.54(7)	O(1)#1-Mn(1)-O(3)	87.07(7)
O(1)#2-Mn(1)-O(2)	109.54(7)	O(1)#2-Mn(1)-O(3)	94.64(8)
O(1)#1-Mn(1)-O(3)#3	94.64(8)	O(2)-Mn(1)-O(3)	87.45(5)
O(1)#2-Mn(1)-O(3)#3	87.07(7)	O(3)#3-Mn(1)-O(3)	174.90(10)
III			
O(1)#1-Mn(1)-O(1)	156.15(7)	O(2)-Mn(1)-O(3)#1	151.29(13)
O(1)#1-Mn(1)-O(1)#2	114.80(13)	O(3)#3-Mn(1)-O(3)#1	94.94(12)
O(1)-Mn(1)-O(1)#2	83.11(13)	Mn(1)#4-O(1)-Mn(1)	125.56(16)
O(1)#1-Mn(1)-O(2)	78.22(13)	Mn(1)#4-O(1)-Mn(1)#2	102.11(13)
O(1)-Mn(1)-O(2)	89.13(13)	Mn(1)-O(1)-Mn(1)#2	96.89(13)
O(1)#2-Mn(1)-O(2)	83.08(13)	Mn(1)#4-O(1)-H(10)	104(3)
O(1)#1-Mn(1)-O(3)#3	79.21(12)	Mn(1)-O(1)-H(10)	117(3)
O(1)-Mn(1)-O(3)#3	85.89(12)	Mn(1)#2-O(1)-H(10)	110(3)

O(1)#2-Mn(1)-O(3)#3	163.96(12)	Mn(1)#3-O(3)-Mn(1)#4	96.03(12)
O(2)-Mn(1)-O(3)#3	108.45(13)	O(1)-Mn(1)-O(3)#1	109.43(13)
O(1)#1-Mn(1)-O(3)#1	90.47(13)	O(1)#2-Mn(1)-O(3)#1	77.87(12)

Symmetry operations used to generate equivalent atoms for **I**: #1 x,-y+1/2,z-1/2 #2 -x,-y,-z+1; for **II**: #1 x,-y+1,z-1/2 #2 -x+1,-y+1,-z+2 #3 -x+1,y,-z+3/2; for **III:** #1 -x+1,y+1/2,-z+1/2 #2 -x+1,-y,-z #3 -x+1,-y,-z+1 #4 -x+1,y-1/2,-z+1/2

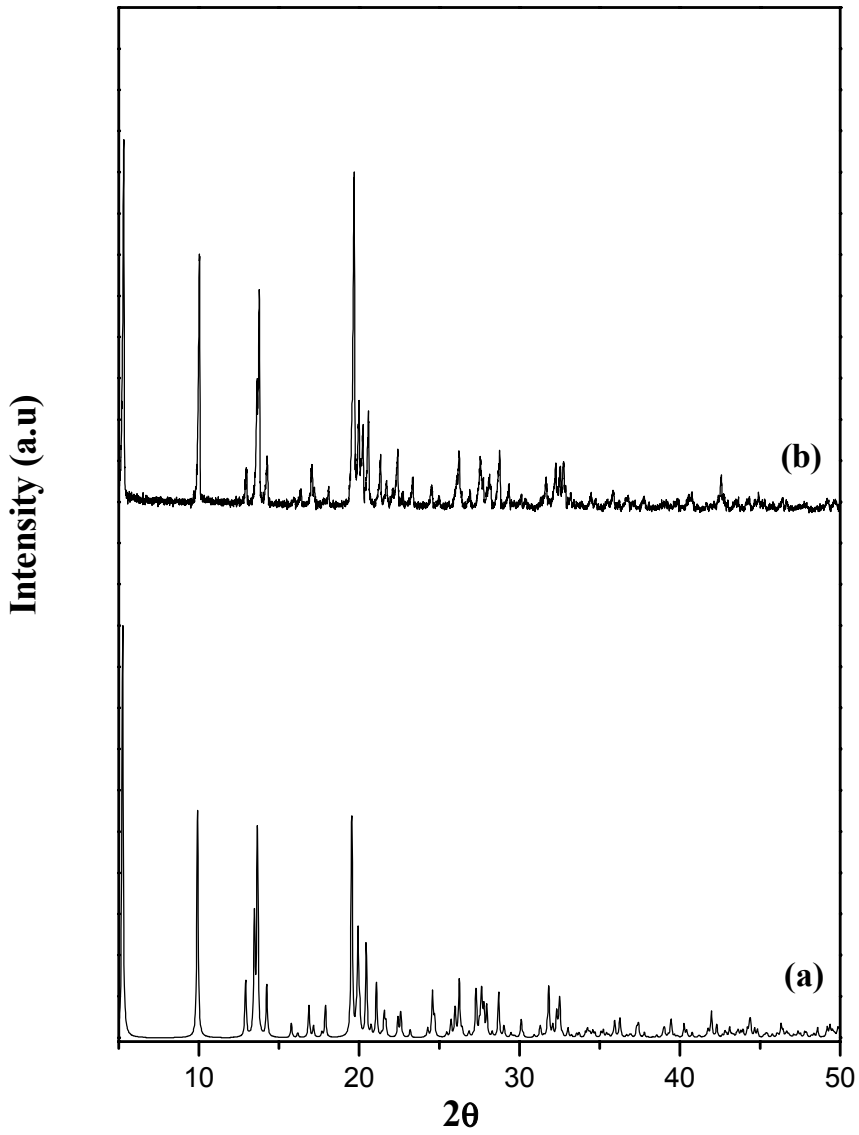

Fig. S1: Powder XRD (CuKα) pattern of **I**, (a) simulated and (b) experimental

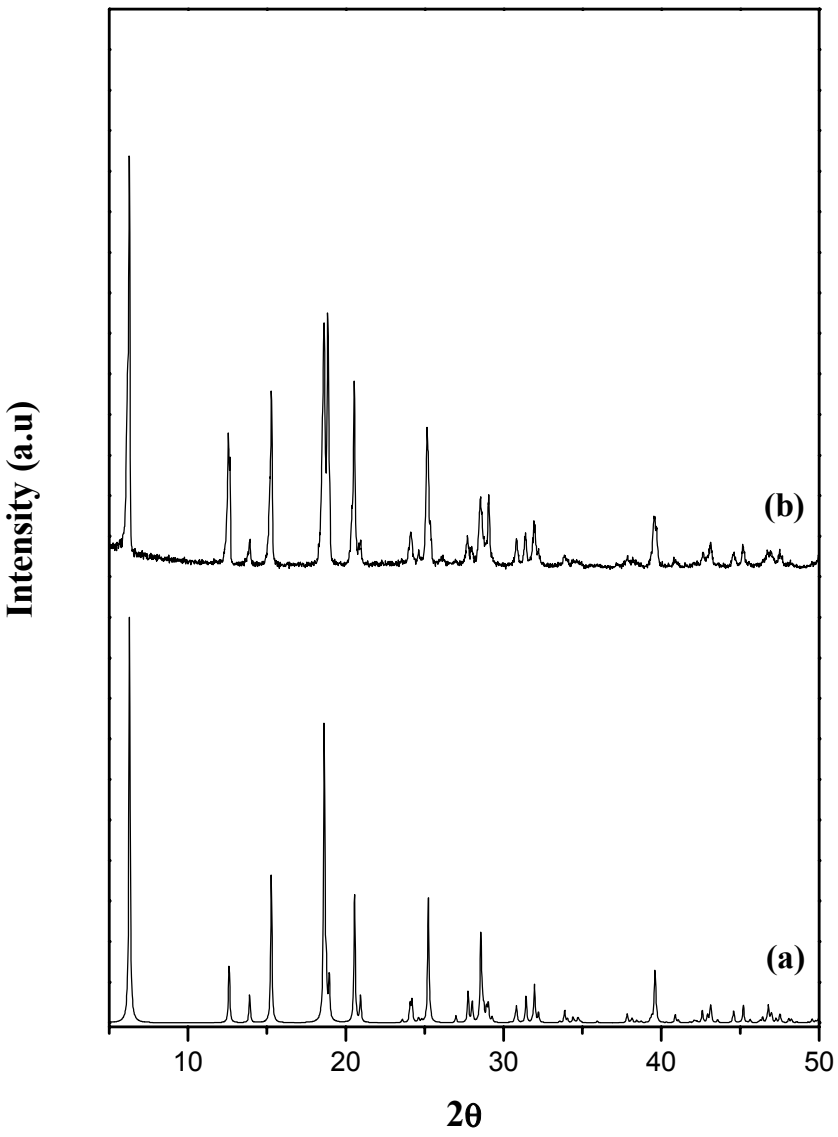

Fig. S2: Powder XRD (CuKα) pattern of **II**, (a) simulated and (b) experimental

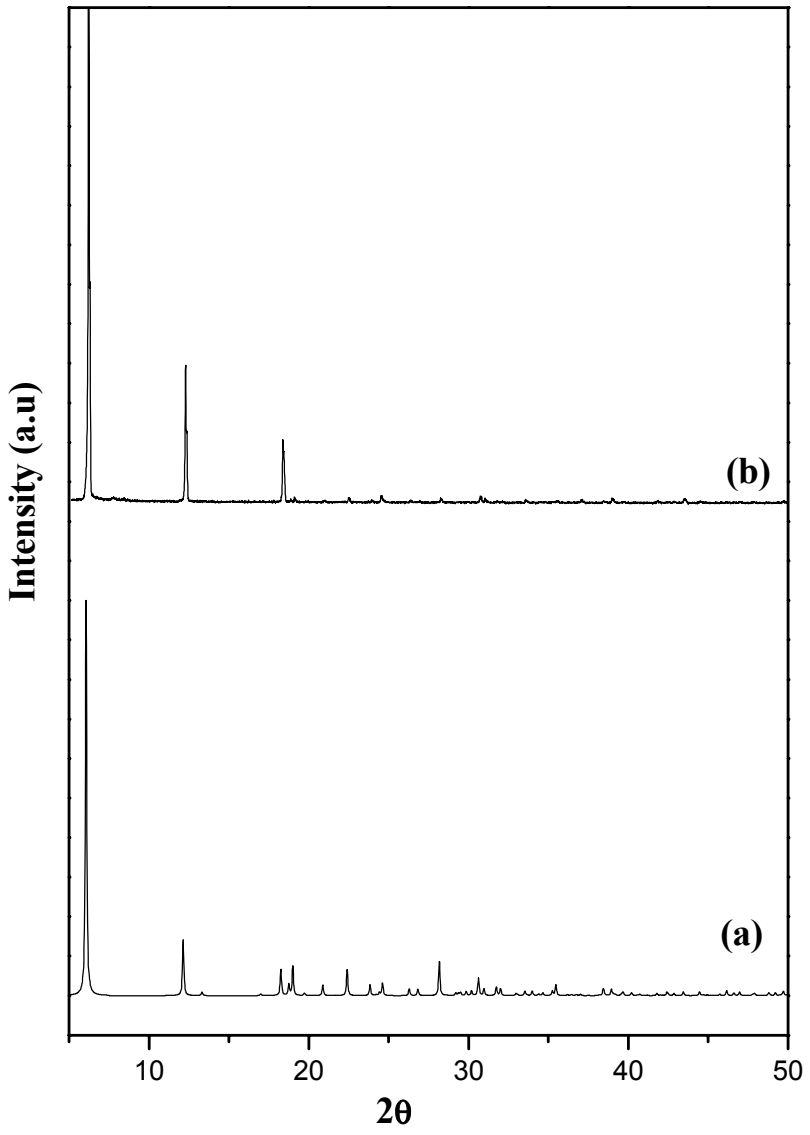

Fig. S3: Powder XRD (CuKα) pattern of **III**, (a) simulated and (b) experimental

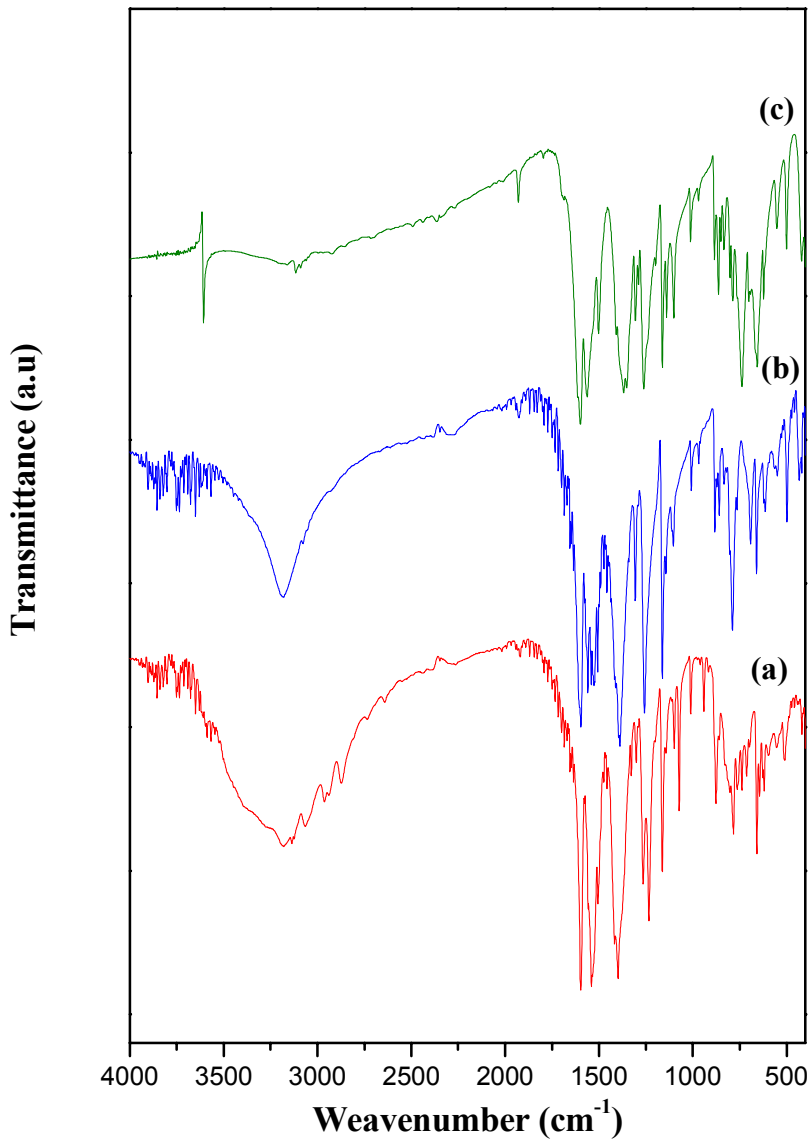

Fig. S4: IR spectra of (a) **I**, (b) **II** and (c) **III**

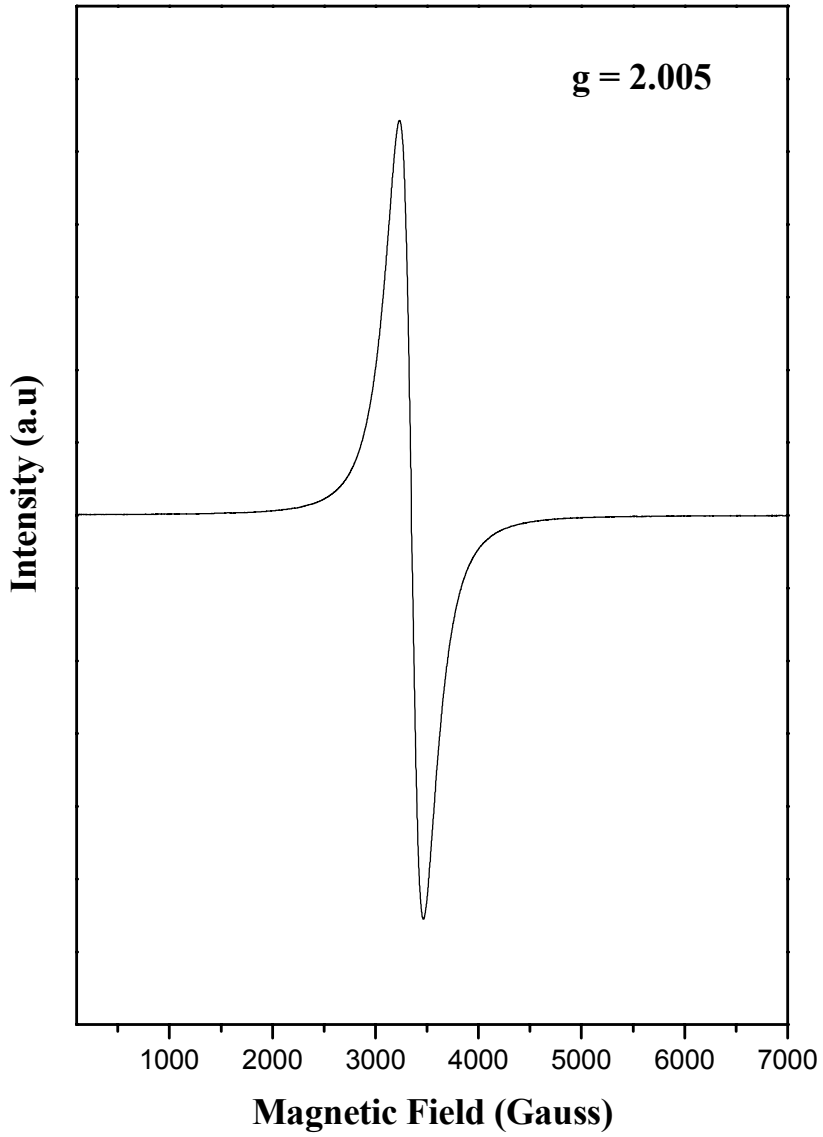

Fig. S5: EPR spectra of **I**

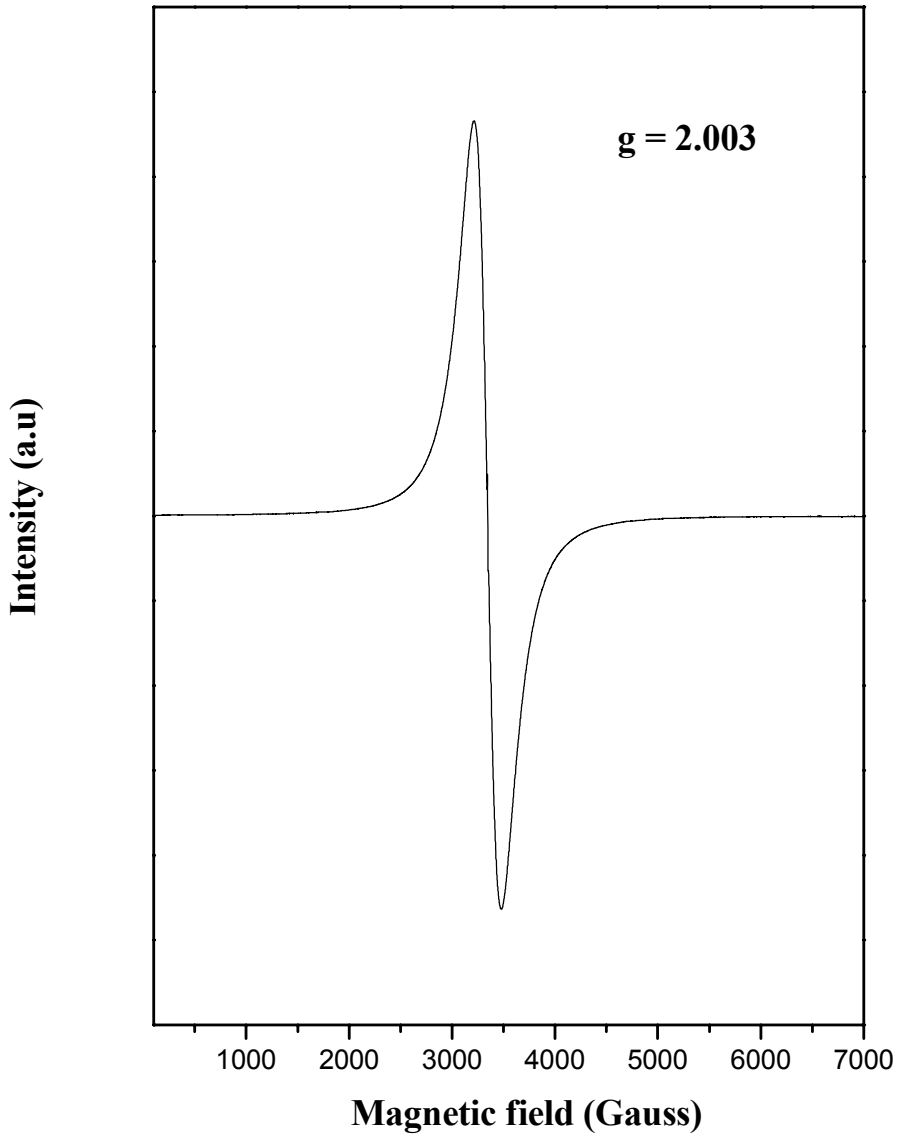

Fig. S6: EPR spectra of **II**

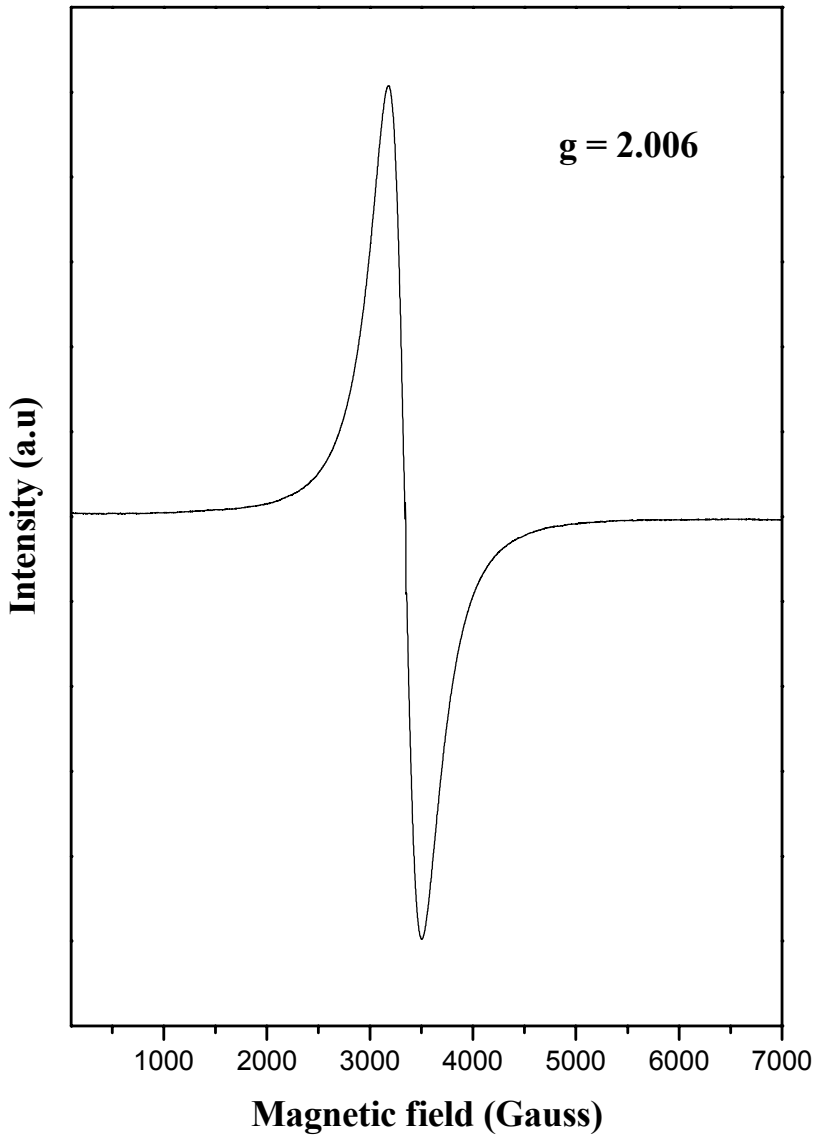

Fig. S7: EPR spectra of **III**

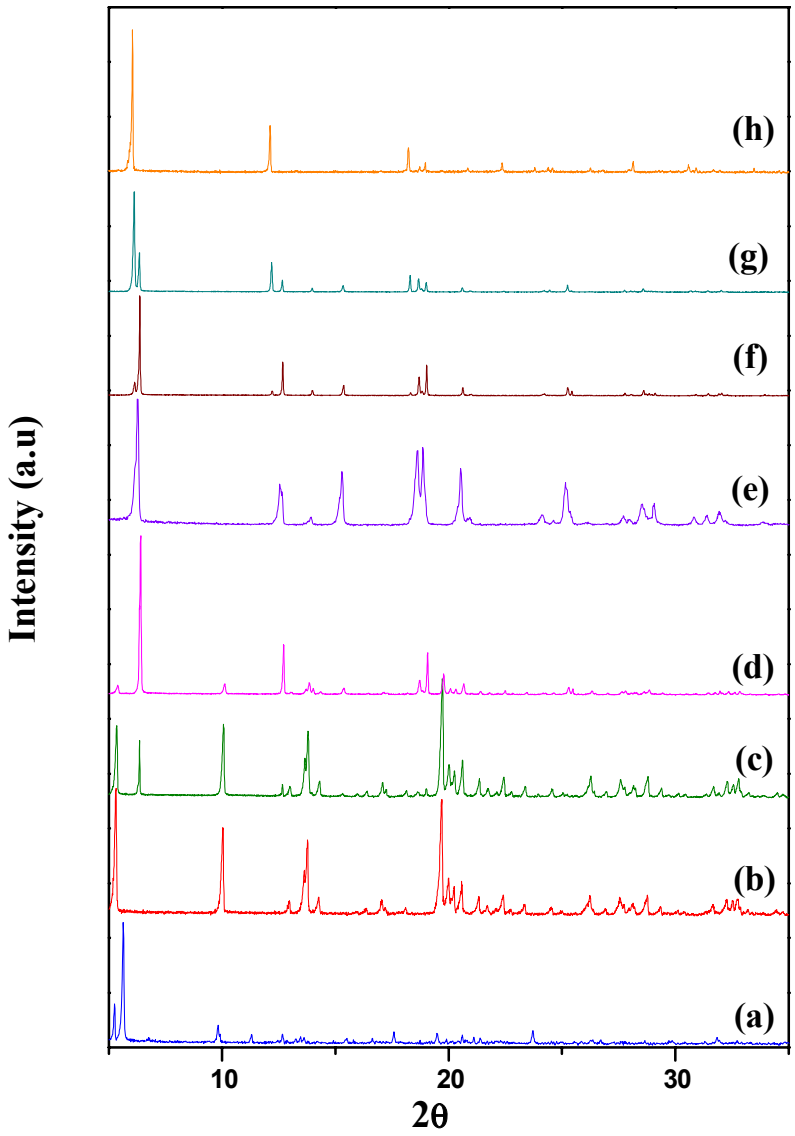

Fig. S8: Powder XRD pattern of the products obtained in different temperature are shown on 5-35 (2θ) scale: (a) 80 (**I** and unknown phase), (b) 100 (pure **I**), (c) 120 (**I** and **II**), (d) 140 (**I** and **II**), (e) 160 (pure **II**), (f) 180 (**II** and **III**), (g) 200 (**II** and **III**) and (h)220 (pure **III**) in ºC.

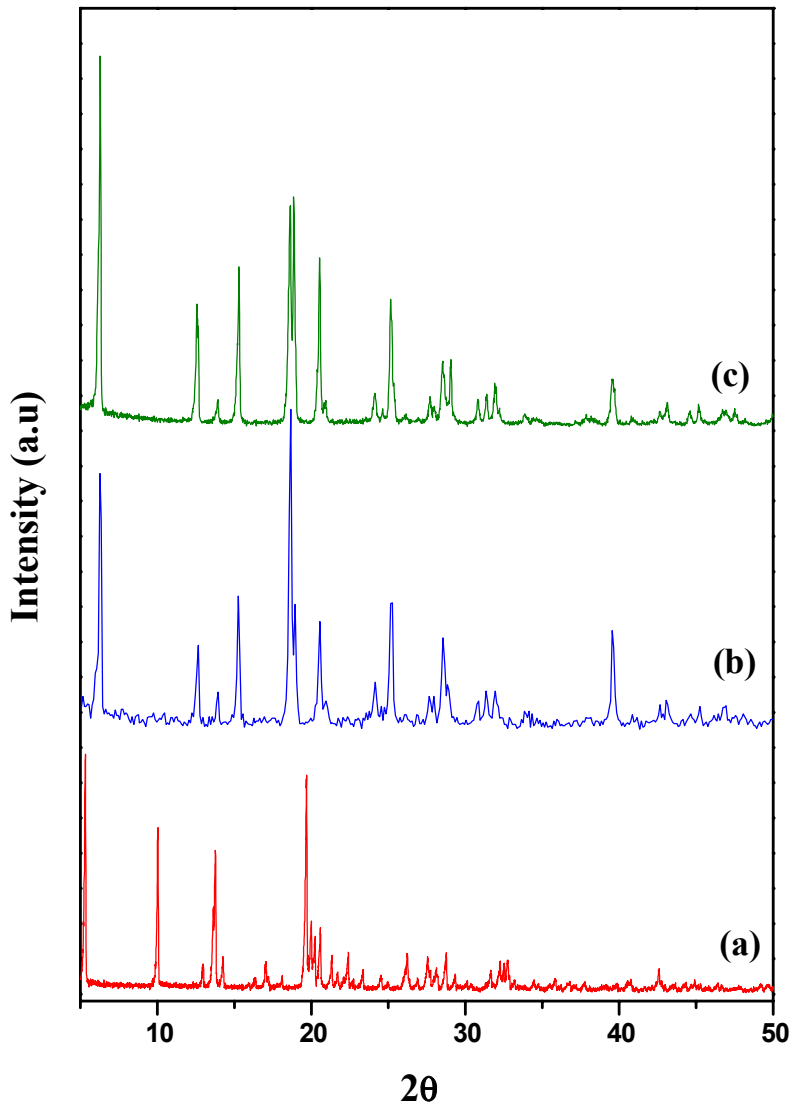

Fig. S9: (a) Powder XRD pattern of the original pure **I**, (b) Powder XRD pattern of the product obtained by heating compound **I** with water in hydrothermal autoclave at 160 º for 24 h, (c) Powder XRD pattern of the original pure **II**. This study indicates that **I** converted completely to **II** through hydrothermal route.

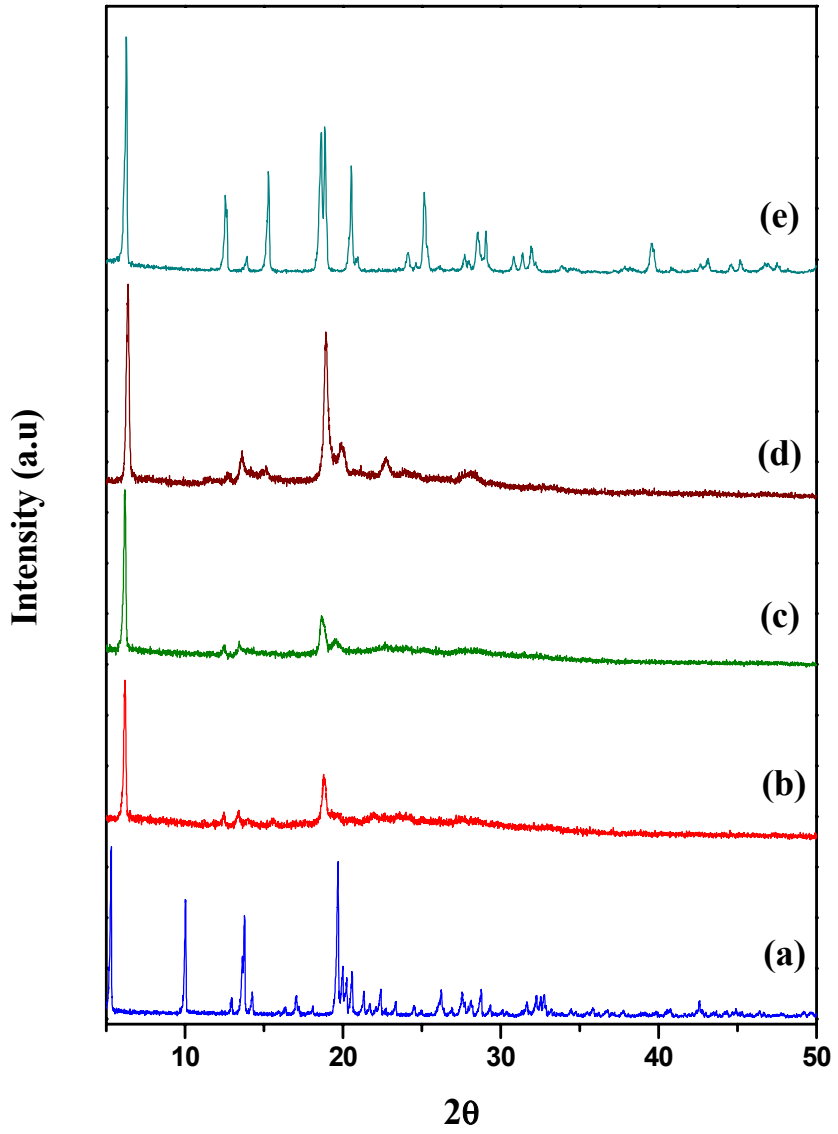

Fig. S10: (a) Powder XRD pattern of the original pure **I**, (b) Powder XRD pattern of the product obtained by heating compound **I** in air at 160 ºC for 2h, (c) Powder XRD pattern of the product obtained by heating compound **I** in air at 160 ºC for 4h, (d) Powder XRD pattern of the product obtained by heating compound **I** in air at 160 ºC for 8h, (e) Powder XRD pattern of the original pure **II**. This study indicates that **I** converted to a phase related with **II**. But the crystalinity of this product is very poor.

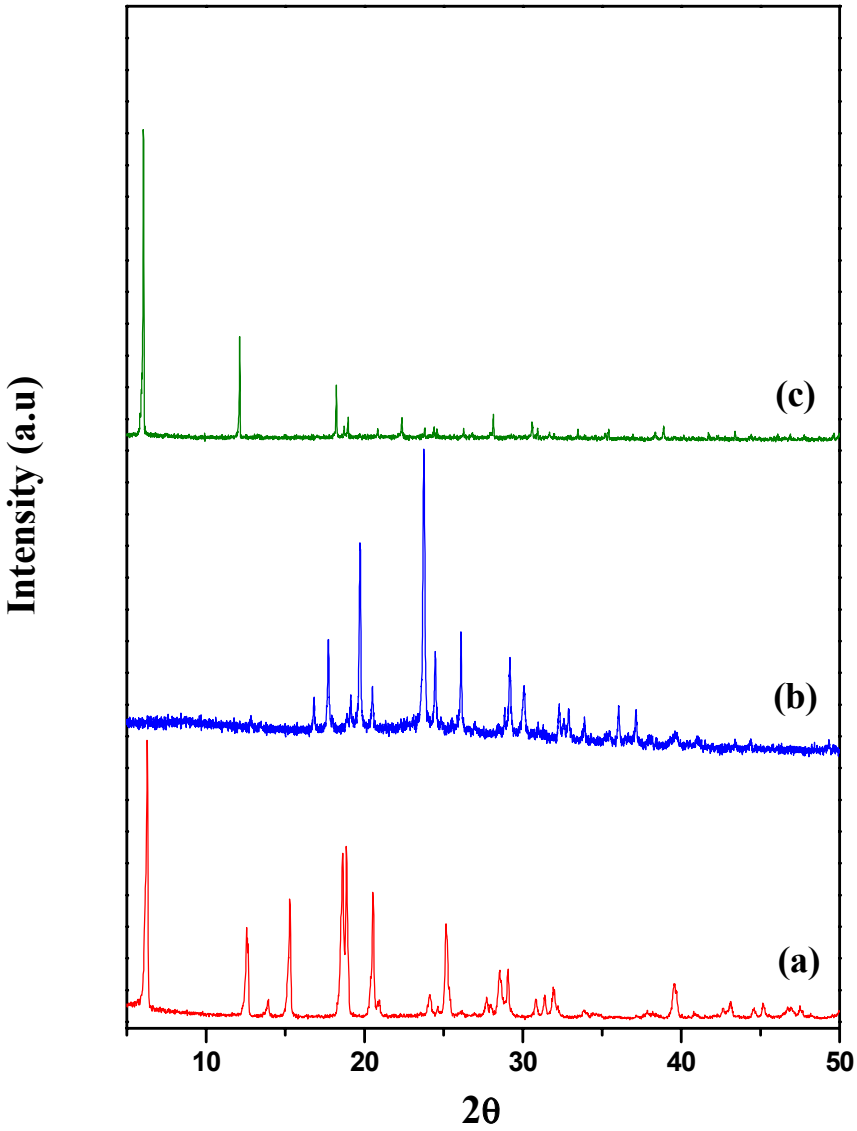

Fig. S11: (a) Powder XRD pattern of the original pure **II**, (b) Powder XRD pattern of the product obtained by heating compound **II** with water in hydrothermal autoclave at 220 º for 24 h, (c) Powder XRD pattern of the original pure **III**. This study indicates that **II** did not convert to **III** through the simple heating in presence of water (hydrothemally).

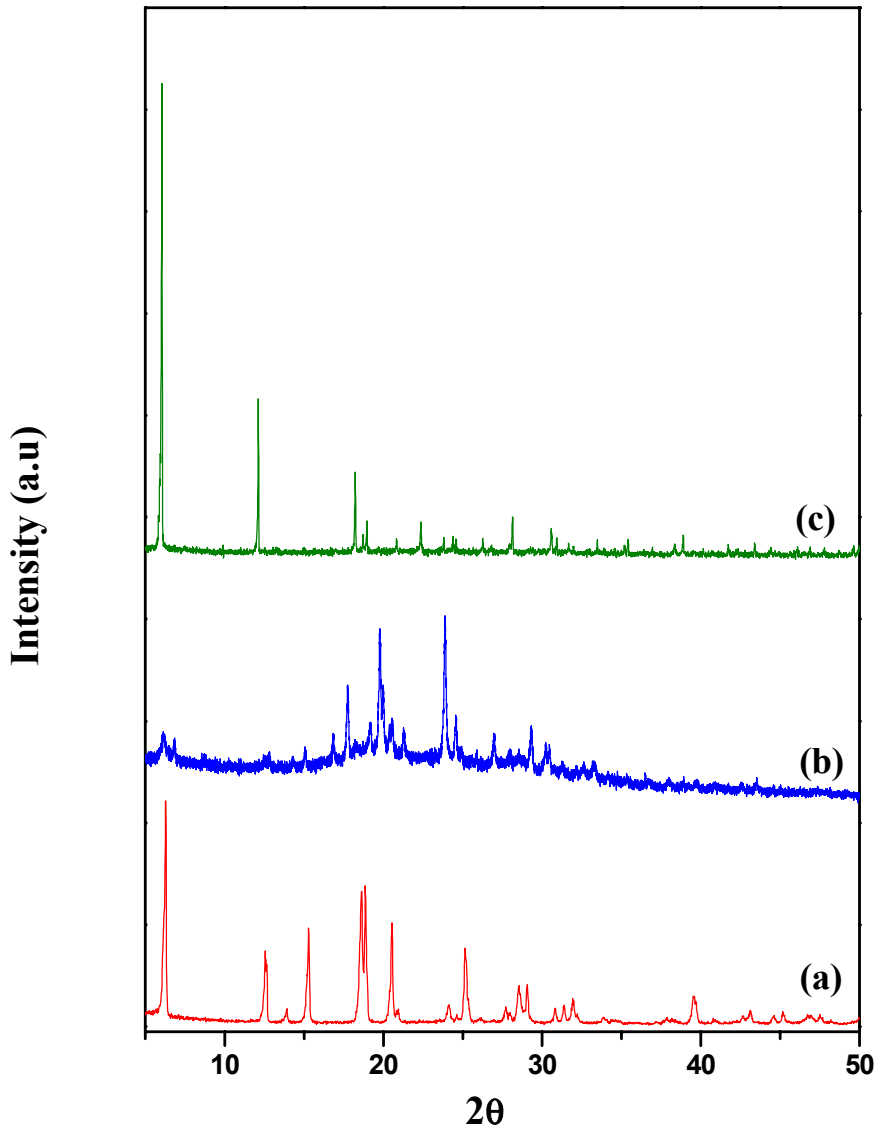

Fig. S12: (a) Powder XRD pattern of the original pure **II**, (b) Powder XRD pattern of the product obtained by heating compound **I** in air at 220 ºC for 2h, (c) Powder XRD pattern of the original pure **III**. This study indicates that **II** did not convert to a phase related with **III** through the heating in air.

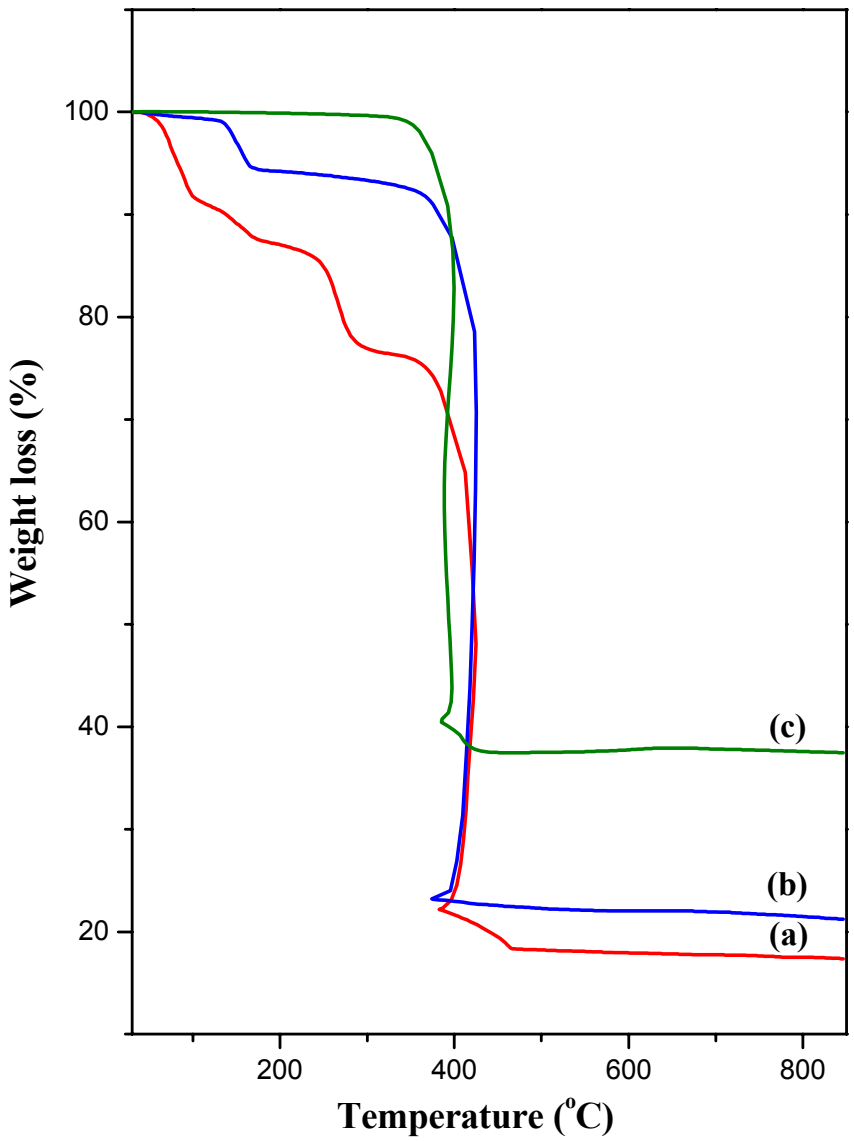

Fig. S13: TGA studies (in air) of (a) **I**, (b) **II** and (c) **III**. The PXRD Pattern of the final decomposed product corresponds to Mn_2O_3 in all the cases (JCPDS No. 78-0390). The total observed weight loss correspond well with the loss of water molecules and the decomposition of the carboxylate ligand for all the three compounds. For **I**: observed – 82%, calculated – 79.4%; for **II**: observed – 78%, calculated – 78.02%, for **III**: observed – 62%, calculated – 60.5%. As a special mention for the compound **II**, the 13% (calc 14%) weight loss upto 175 ºC indicate the loss of three water molecules as well as the transformation from $[\{Mn(H_2O)_3\}\{C_{12}H_8O(COO)_2\}].H_2O$, **I**, to $[\{Mn(H_2O)\}\{C_{12}H_8O(COO)_2\}]$, **II**.

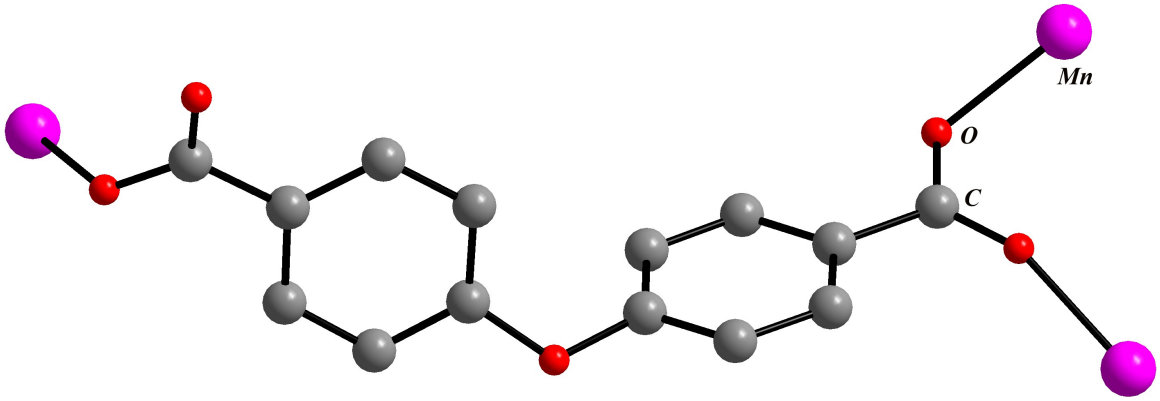

(a)

(b)

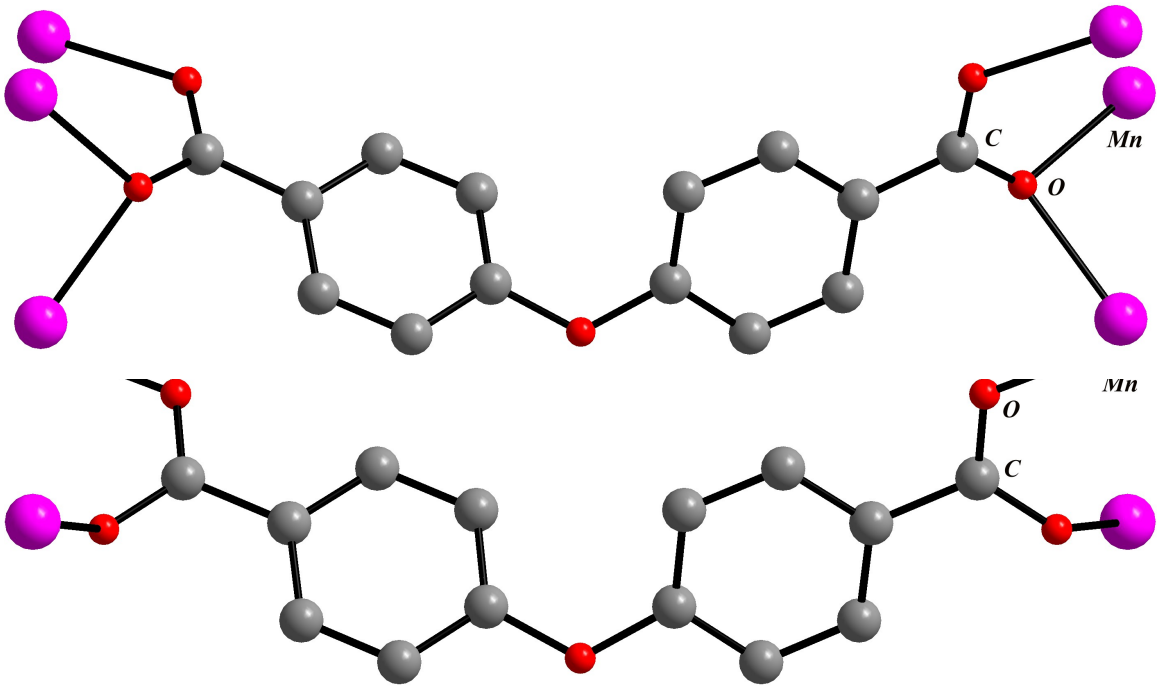

(c)

Fig. S14: The coordination mode of oxy-bis(benzoate) (OBA) (a) **I** (one OBA coordinating with three Mn^{+2} ions), (b) **II** (one OBA coordinating with four Mn^{+2} ions) and (c) **III** (one OBA coordinating with six Mn^{+2} ions).

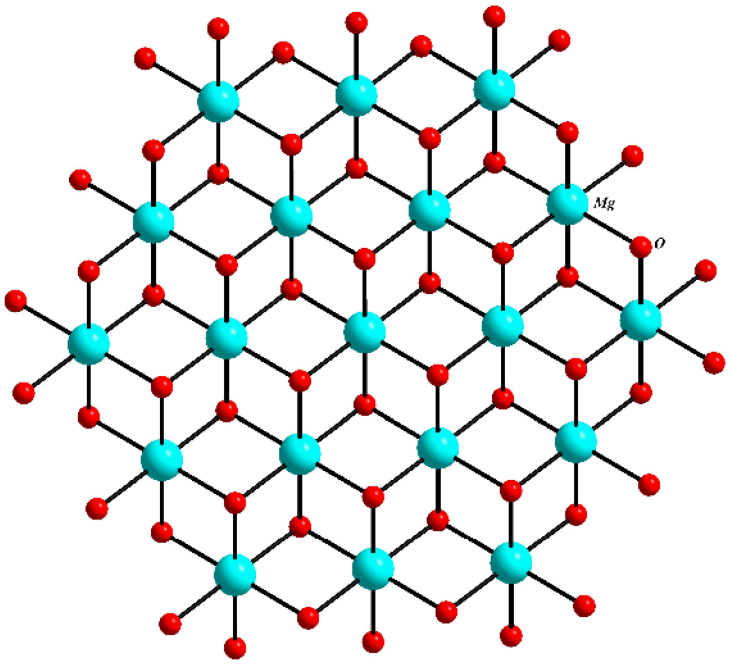

(a)

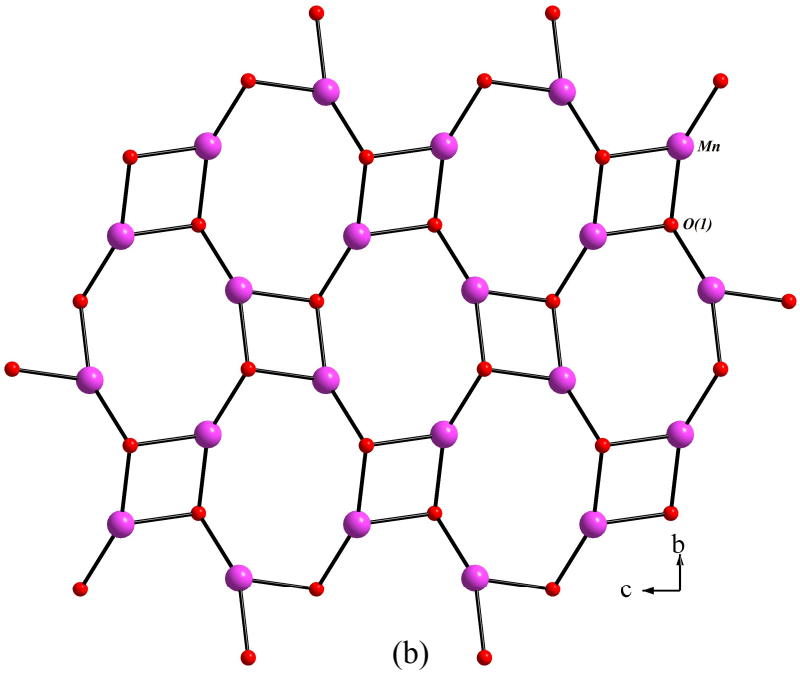

(b)

Fig. S15: (a) Structure of $M(OH)_2$ (M = bivalent ions) brucite layer, where all the connectivity between MO_6 octahedra are identical, (b) Structure of Mn(OH) layer observed in[$\{Mn(OH)\}_2\{C_{12}H_8O(COO)_2\}$], **III** (carboxylate oxygens are not shown). Note that half the –OH groups have been removed from the perfect brucite layer.

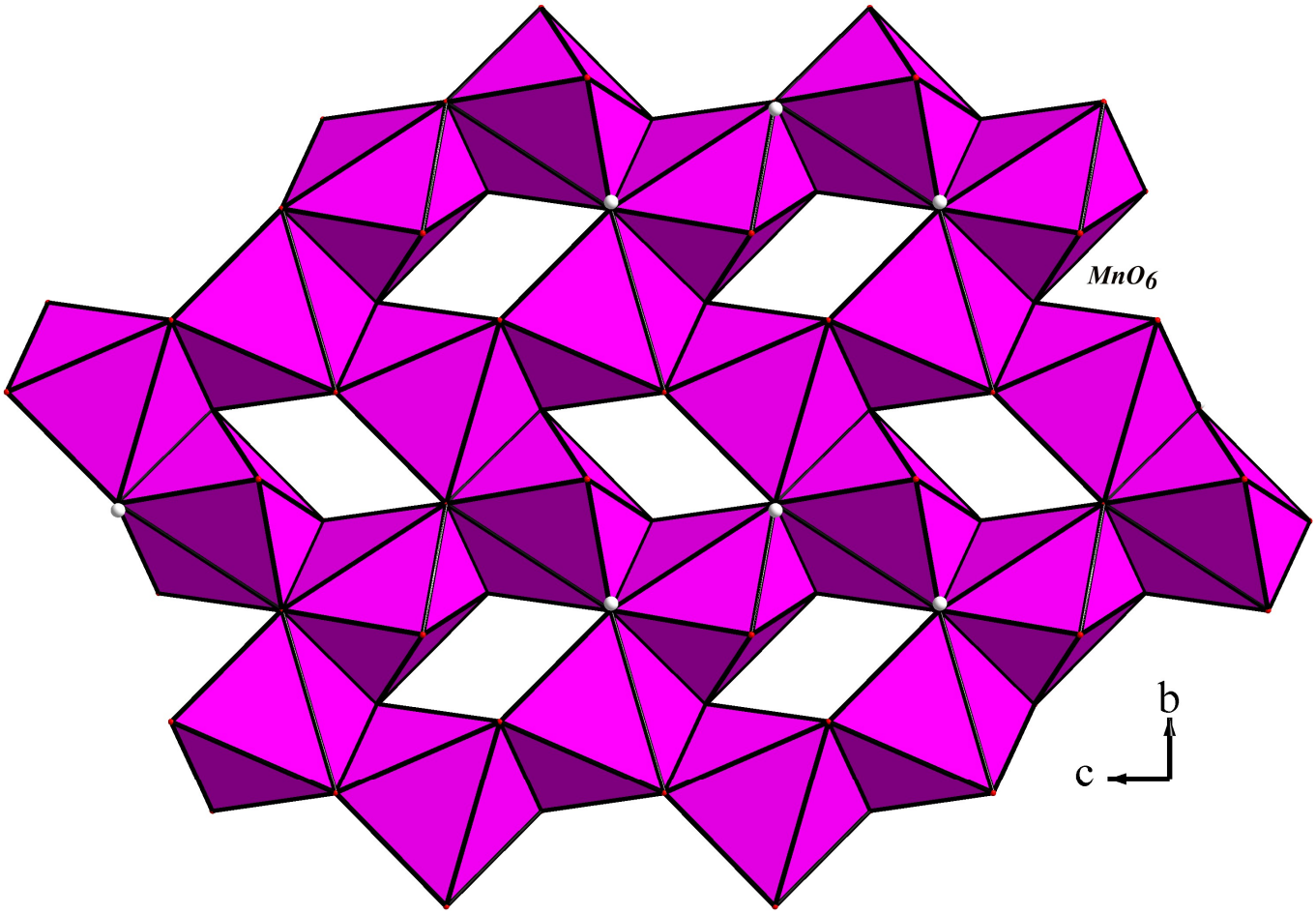

Fig. S16: (a) Polyhedral view of the layer in [{Mn(OH)}$_2${$C_{12}H_8O(COO)_2$}], **III**. Note that the MnO_6 polyhedra are have three edge shared and two corner shared octahedral.

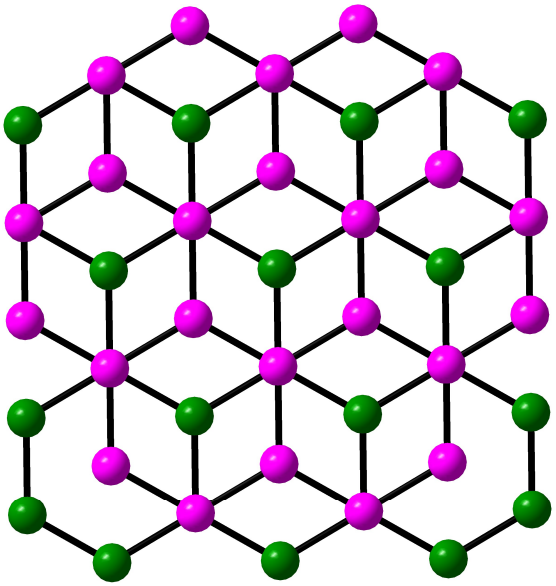

(a)

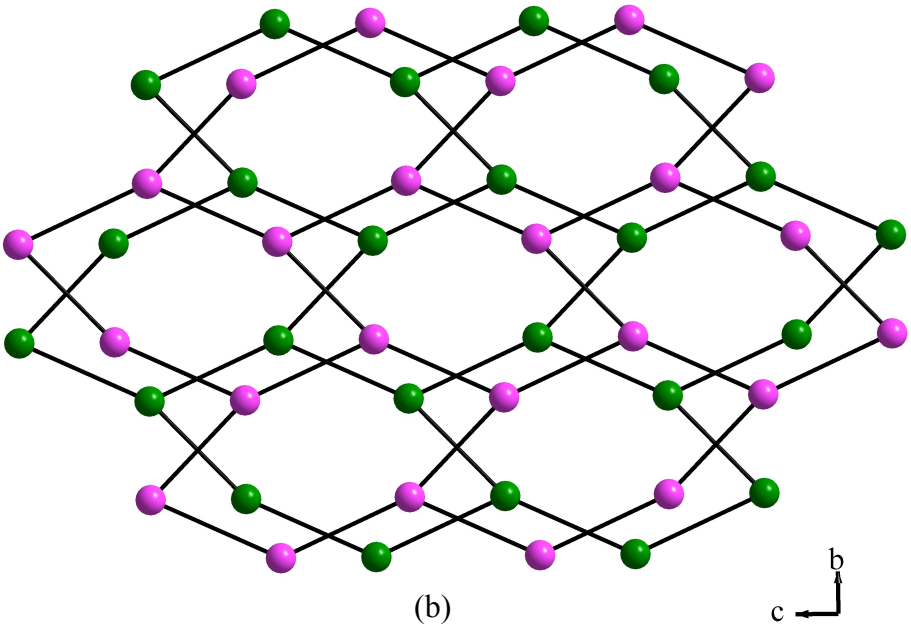

(b)

Fig. S17: (a) Arrangement of layer in pure graphite in ABAB…fashion, where purple color represent 'C' atom of layer 1 and green color represent 'C' atom of layer 2, (b) Arrangement of Mn-Mn units within one layer in $[\{Mn(OH)\}_2\{C_{12}H_8O(COO)_2\}]$, **III,** where pink color represent 'Mn' atom of layer 1 and green color represent 'Mn' of layer 2. Note that in both the cases layers are arranged in ABAB…fashion.

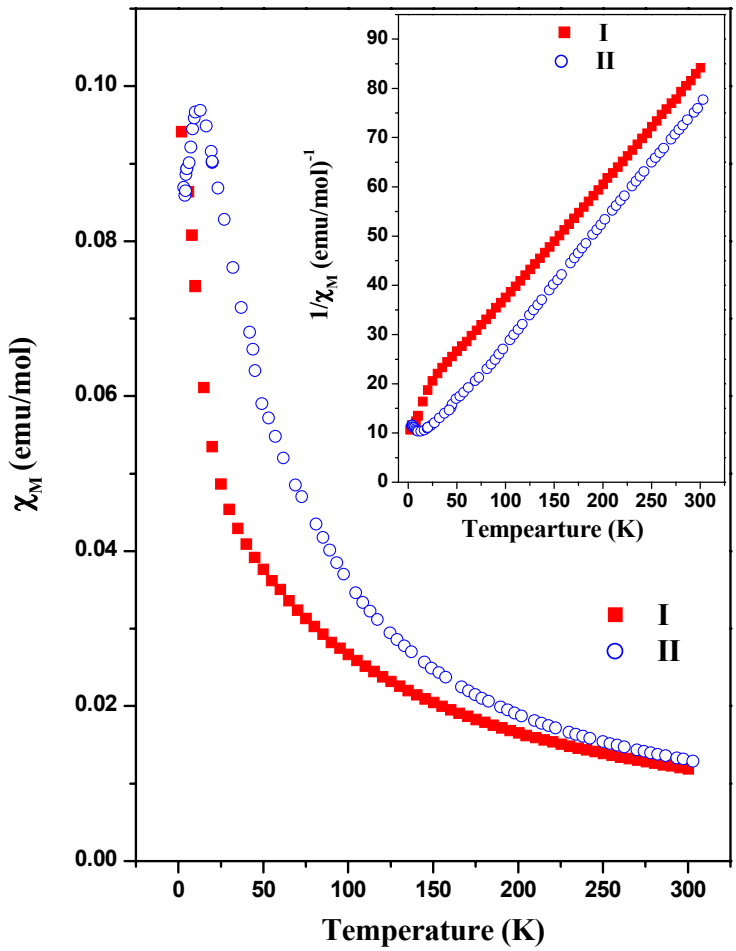

Fig. S18: (a) Figure shows the thermal variation of the molar susceptibility (χ_M) for **I** and **II** under ZFC condition (H = 1000 Oe). Inset shows the thermal variation of the inverse molar susceptibility ($1/\chi_M$) (ZFC). At RT, the observed effective magnetic moment is 5.55 and 5.61 μ_B, respectively for **I** and **II,** which are slightly lower than the spin only value for Mn^{+2} (5.92 μ_B). While **I** does not show any magnetic ordering down to 2K, **II** shows anti-ferromagnetic behavior with a T_N = 12 K. The high temperature magnetic susceptibility data (100-300K) can be fitted to the Curie-Weiss behavior with C = 4.30 and 2.42 emu/mol and θ_P = -60.2 and -14.2 K, respectively for **I** and **II**. The negative Weiss constant in both the compound indicate anti-ferromagnetic behavior

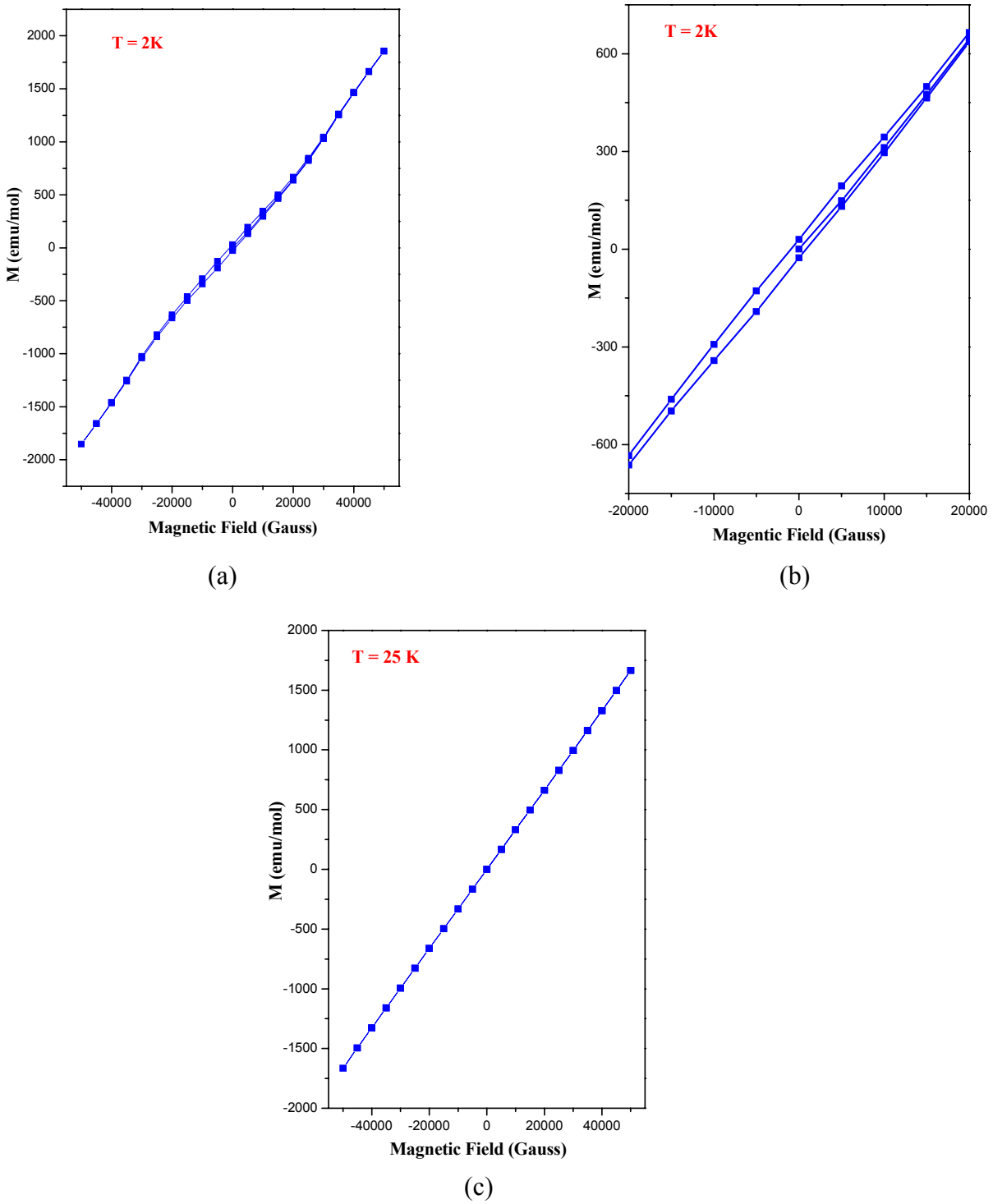

Fig. S19: The M *Vs* H behavior of $[\{Mn(OH)\}_2\{C_{12}H_8O(COO)_2\}]$, **III** (a) at 2 K, (b) at 2 K in lower field (0-20000 Oe) and (c) at 25 K.

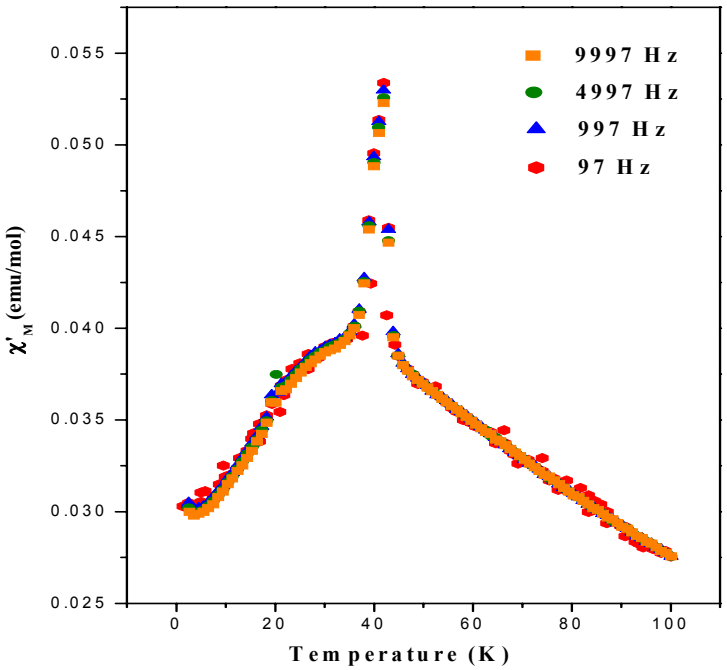

(a)

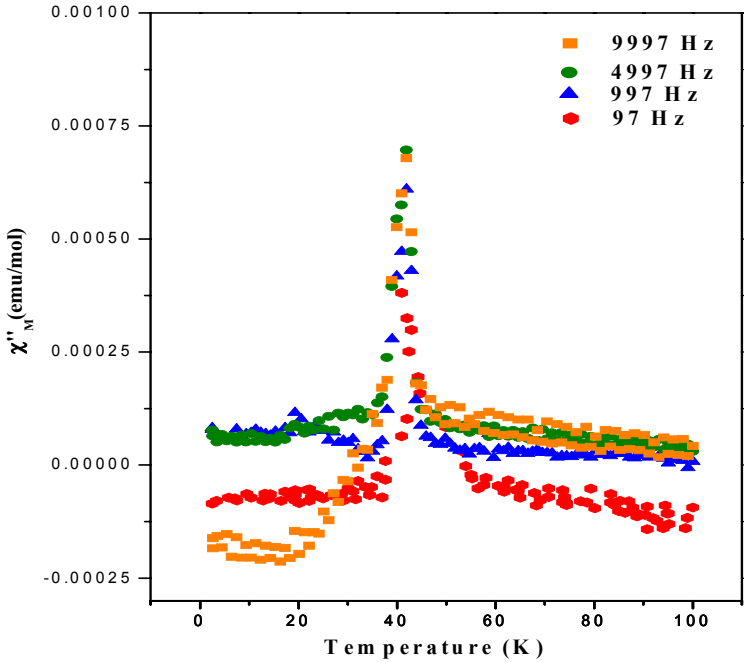

(b)

Fig. S20: Frequency dependence of the AC molar magnetic susceptibility of $[\{Mn(OH)\}_2\{C_{12}H_8O(COO)_2\}]$, **III** (a) in-phase signal, (b) out-of-phase signal. Note the peak of both cases at 42 K.